Phase Transitions and Superconductivity

RQEMP 2005 (Hilke@physics.mcgill.ca)

- Temperature driven Phase transitions (normal-to-superconductor transitions)
- Phase transitions of vortices
- Quantum Phase Transitions:
  - – Disorder induced transitions
  - – Interaction induces transitions

"Taste" of a phase transition

Figure 1. Good and bad chocolate: The well-tempered chocolate on top is glossy and has come away easily from the mold. The untempered chocolate sticks in the mold and shows a spotted and marked surface typical of strong fat "bloom."

The Materials Science of Chocolate

Peter Fryer and Kerstin Pinschower

Table II: Overview of Cocoa-Butter Polymorphs.

Polymorph	Conditions under which Polymorph Arises	Melting Point (°C)	Comments
Form I	Rapid cooling of melt. (Successive polymorphs are then obtained sequentially by heating at 0.5°C min^{-1}.)	17.3	
Form II	Cooling of melt at 2°C min. Rapid cooling of melt, followed by storing from several min up to 1 h at 0°C. The form is stable at 0°C for up to 5 h.	23.3	
Form III	Solidification of melt at 5–10°C. Transformation of Form II by storing at 5–10°C.	25.5	
Form IV	Solidification of melt at 16–21°C. Transformation of Form III by storing at 16–21°C.	27.3	
Form V	Solidification of melt. Transformation of Form IV. Solvent crystallization.	33.8	Forms after tempering, has good gloss and texture; most desirable form.
Form VI	Transformation of Form V (4 months at room temperature).	36.3	"Bloomed" chocolate.

Chocolate

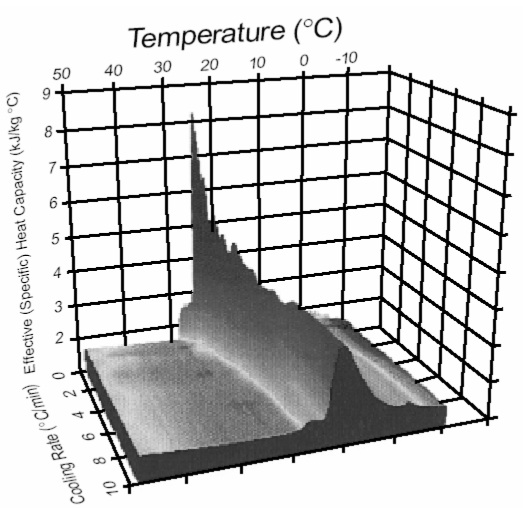

Figure 3. Effective (specific) heat capacity of milk chocolate as a function of temperature and cooling rate. Data obtained using differential scanning calorimetry. (From Reference 16.)

Water-ice

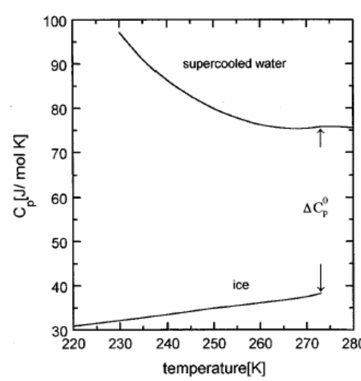

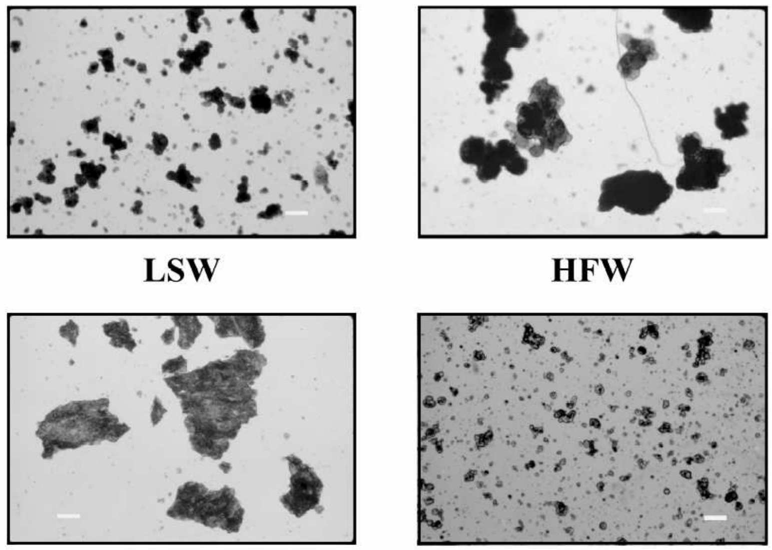

Figure 1. Optical micrographs of milk powders (LSN: spray-dried skim milk powder; LSW: spray-dried whole milk powder; RDW: roller-dried whole milk powder; HFW: skim milk powder dried with cream in fluidized bed).

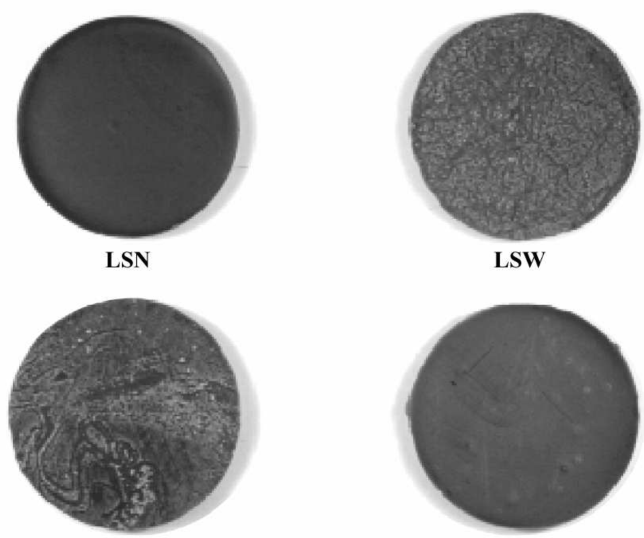

9-week storage, temperature fluctuation (19-29^{o}C)

Figure 4. Bloom formation in milk chocolates made with different milk powders after storage for 9 wk with temperature fluctuating between 19 and 29°C every 6 h (LSN: spray-dried skim milk powder; LSW: spray-dried whole milk powder; RDW: roller-dried whole milk powder; HFW: skim milk powder dried with cream in fluidized bed).

Gas-Liquid-Solid: First and Second Order Phase Transitions

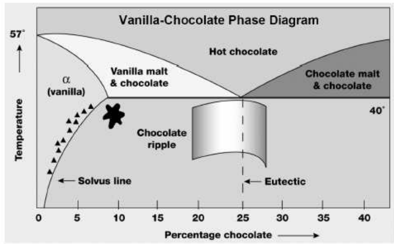

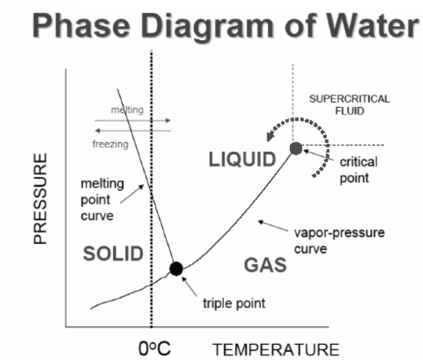

Unusual phase diagram- the solid/liquid equilibrium line slopes left

Superconductivity

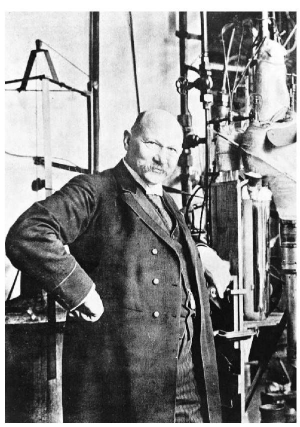

Kamerlingh Onnes, 1911

perfect conductivity

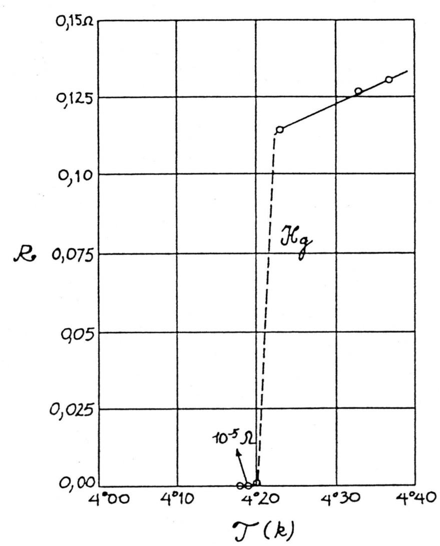

Gap determination by tunneling

Nobel 1973

VOLUME 5, NUMBER 4 PHYSICAL REVIEW LETTERS AUGUST 15, 1960

ENERGY GAP IN SUPERCONDUCTORS MEASURED BY ELECTRON TUNNELING

Ivar Giaever
General Electric Research Laboratory, Schenectady, New York
(Received July 5, 1960)

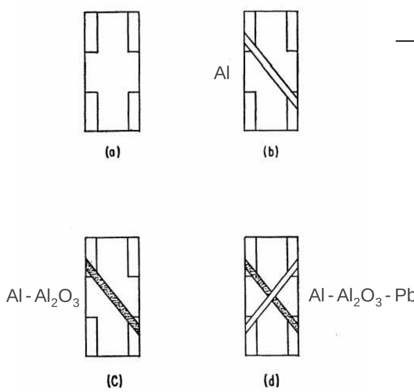

FIG. 3. Sample preparation. (a) Glass slide with indium contacts. (b) An aluminum strip has been deposited across the contacts. (c) The aluminum strip has been oxidized. (d) A lead film has been deposited across the aluminum film, forming an Al-Al_2O_3-Pb sandwich.

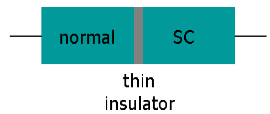

Tunneling experiments

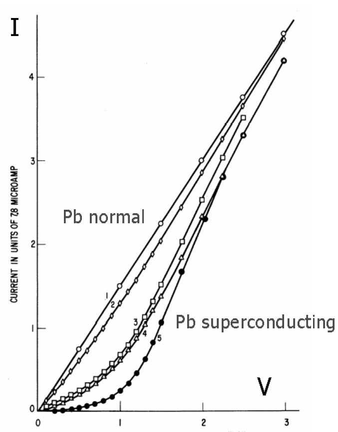

FIG. 1. Tunnel current between Al and Pb through Al_2O_3 film as a function of voltage. (1) $T = 4.2°K$ and $1.6°K$, $H = 2.7$ koe (Pb normal). (2) $T = 4.2°K$, $H = 0.8$ koe. (3) $T = 1.6°K$, $H = 0.8$ koe. (4) $T = 4.2°K$, $H = 0$ (Pb superconducting). (5) $T = 1.6°K$, $H = 0$ (Pb superconducting).

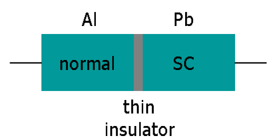

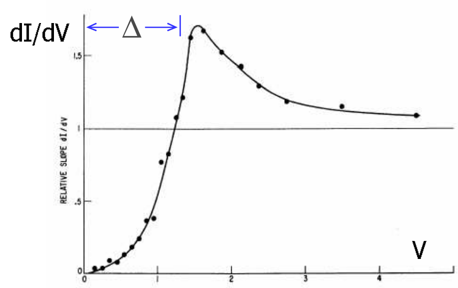

FIG. 2. From Fig. 1, slope dI/dV of curve 5 relative to slope of curve 1.

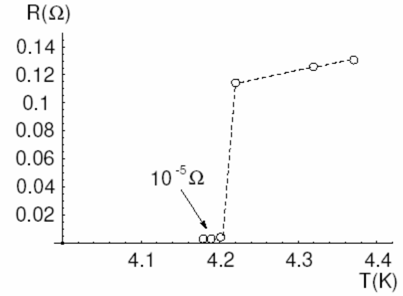

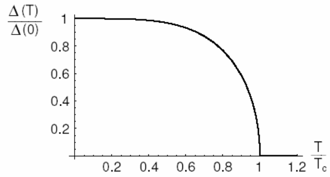

FIG. 3 *The gap vs. temperature in Al as determined by electron tunneling.*

e.m. absorption (Glover and Tinkham, 1956)

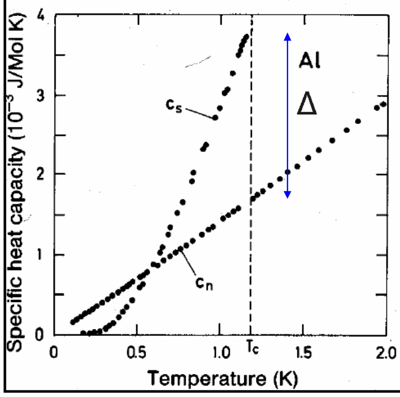

What's the order parameter?

Analogy to Ferromagnetic transition: Order Parameter=Magnetization

1. T=0

well ordered

2. 0<T<Tc

ordered

3. T>Tc

disordered

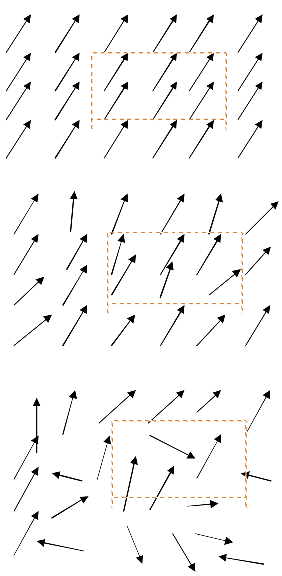

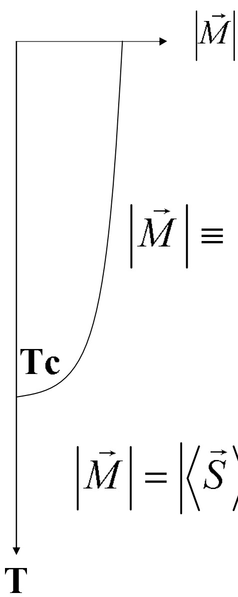

$$\left|\vec{M}\right| \equiv \left|\left\langle \vec{S} \right\rangle\right| > 0$$

$$\left|\vec{M}\right| = \left|\left\langle \vec{S} \right\rangle\right| = 0$$

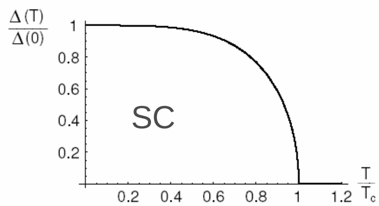

FIG. 3 *The gap vs. temperature in Al as determined by electron tunneling.*

Δ is the order parameter: → continuous phase transition

Mean-field (Landau) theory of continuous phase transitions

Approximate free energy close to phase transition:

$$F = \int d^D x \left[\vec{\nabla}\phi^* \vec{\nabla}\phi + a(T)\phi^*\phi + \frac{b(T)}{2}(\phi^*\phi)^2 \right]$$

Higher order terms $(\nabla\phi^*\nabla\phi)^2, (\phi^*\phi)^3, \ldots$

are expected to be smaller close enough to Tc. Expand around Tc:

$$\begin{cases} a(T) = \alpha(T - T_c) + \ldots, \\ b(T) = \beta + \ldots \end{cases}$$

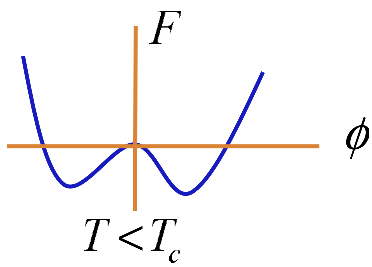

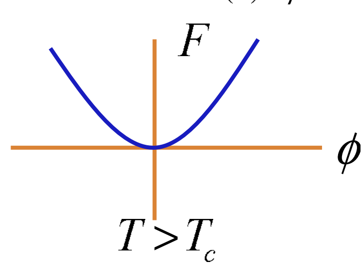

Ginzburg–Landau:

Order parameter:

The complex order parameter is "amplitude of the Cooper pair center of mass":

$$\Psi(x) \propto \Delta(x), \quad \Delta(k) \propto \left\langle c_{\uparrow}(k) c_{\downarrow}(-k) \right\rangle$$

which is "the gap function". $\Psi(x) \equiv \sqrt{n_s{}^*(x)}\, e^{i\phi(x)}$

$n_s{}^*(x) = \dfrac{n_s(x)}{2}$ **density of the Cooper pairs**

$\phi(x)$ **the superconductor U(1) phase**

For B=0, the GL free energy is:

$$F[\Psi] = \int d^3x \left[\frac{\hbar^2}{2m^*} \vec{\nabla}\Psi^* \vec{\nabla}\Psi + \alpha(T - T_c)\,\Psi^*\Psi + \frac{\beta}{2}(\Psi^*\Psi)^2 \right]$$

$$m^* = 2\, m_e$$

For B≠0:

Invariance under local gauge transformations:

$$\begin{cases} \Psi(x) \to e^{i\chi(x)}\Psi(x) \\ \vec{A}(x) \to \vec{A}(x) + \dfrac{\hbar c}{e^*}\vec{\nabla}\chi(x) \end{cases} \qquad e^* = 2e$$

To ensure local gauge invariance one makes the "minimal substitution", namely replaces any derivative by a covariant derivative:

$$\vec{D}\Psi(x) = \left(\vec{\nabla} - i\frac{e^*}{\hbar c}\vec{A}\right)\Psi(x)$$

The local gauge invariance of the gradient term:

$$\vec{D}\Psi(x) \to \left[\vec{\nabla} - \frac{ie^*}{\hbar c}\left(\vec{A} + \frac{c\hbar}{e^*}\vec{\nabla}\chi(x)\right)\right]\Psi(x)e^{i\chi(x)}$$

$$= \left[\vec{\nabla}\Psi + \Psi \cdot i\vec{\nabla}\chi - \frac{ie^*}{\hbar c}\vec{A}\cdot\Psi - i\vec{\nabla}\chi\cdot\Psi\right]e^{i\chi(x)}$$

$$= \vec{D}\Psi \cdot e^{i\chi(x)}$$

$$|\vec{D}\Psi(x)|^2 \to |\vec{D}\Psi(x)|^2$$

Ginzburg – Landau equations:

Minimizing the free energy with covariant derivatives one arrives at the set of GL equations: the nonlinear Schrödinger equation (variation with respect to Ψ)

$$-\frac{\hbar^2}{2m^*}\left(\vec{\nabla} - i\frac{e^*}{\hbar c}\vec{A}\right)^2\Psi + \alpha(T - T_c)\Psi + \beta\Psi\left|\Psi\right|^2 = 0$$

and the supercurrent equation (variation of A):

$$\frac{c}{4\pi}\vec{\nabla}\times\vec{B} = \vec{J}_s \equiv -\frac{ie^*\hbar}{2m^*}(\Psi^*\vec{\nabla}\Psi - \Psi\vec{\nabla}\Psi^*) - \frac{e^{*2}}{m^*c}\left|\Psi\right|^2\vec{A}$$

Two characteristic length scales

Coherence length ξ

characterizes variations of $\Psi(x)$ **, while the penetration depth λ characterizes variations of** $B(x)$

$$\xi(T) = \frac{\hbar}{\sqrt{2m^*\alpha(T_c - T)}},$$

$$\lambda(T) = \frac{c}{e^*}\sqrt{\frac{m^*\beta}{4\pi\alpha\left(T_c - T\right)}}$$

Both diverge at T=Tc.

Ginzburg – Landau parameter:

Temperature independent dimensionless parameter:

$$\kappa = \frac{\lambda(T)}{\xi(T)} = \frac{m^* c}{e^*\hbar}\sqrt{\frac{\beta}{2\pi}}$$

Properties depend on the GL parameter:

$\kappa < \frac{1}{\sqrt{2}}$	$\kappa > \frac{1}{\sqrt{2}}$
Type I	**Type II**

Abrikosov (1957)

Continuous Phase transition and the Ginzburg – Landau Theory

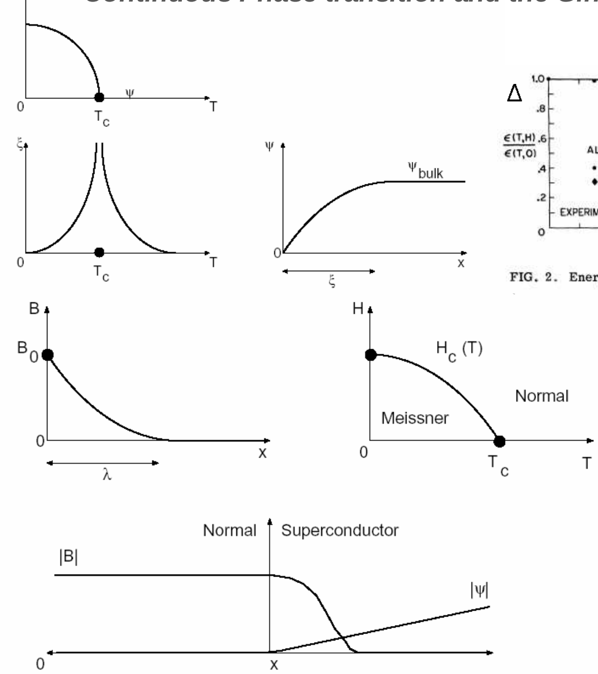

D. H. Douglass, Jr. '61

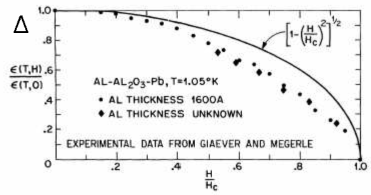

FIG. 2. Energy gap of aluminum vs magnetic field.

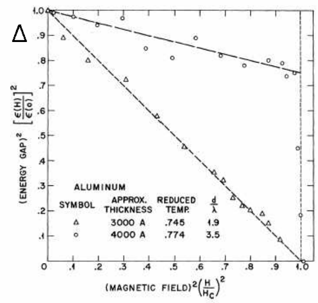

FIG. 1. Energy gap of aluminum vs magnetic field for films of thickness 3000 A and 4000 A. Two other films of thickness 500 A and 2000 A behaved similarly to the 3000A film. The dashed curves are the best straight lines through the data points.

Vortices

A.A. Abrikosov **1957** **2003**

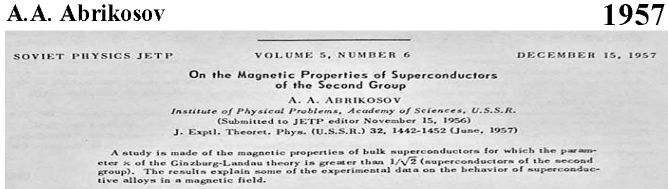

SOVIET PHYSICS JETP VOLUME 5, NUMBER 6 DECEMBER 15, 1957

On the Magnetic Properties of Superconductors of the Second Group

A. A. ABRIKOSOV

Institute of Physical Problems, Academy of Sciences, U.S.S.R.

(Submitted to JETP editor November 15, 1956)

J. Exptl. Theoret. Phys. (U.S.S.R.) 32, 1442-1452 (June, 1957)

A study is made of the magnetic properties of bulk superconductors for which the parameter $\varkappa$ of the Ginzburg-Landau theory is greater than $1/\sqrt{2}$ (superconductors of the second group). The results explain some of the experimental data on the behavior of superconductive alloys in a magnetic field.

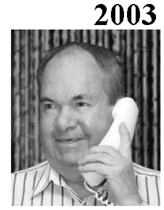

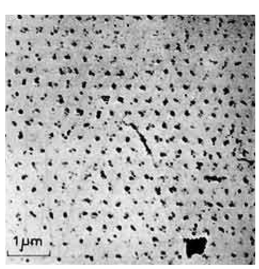

1967
Bitter Decoration

U. Essmann
H. Trauble

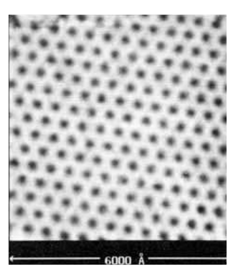

1989
STM

H.F. Hess
Bell labs

Abrikosov vortices in type II superconductors as seen by electron beam tomography.

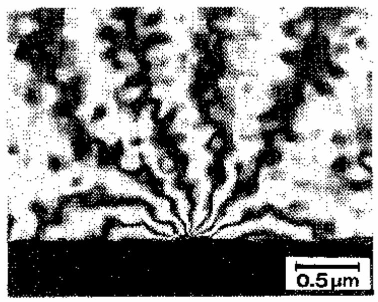

FIG. 2. 16-times phase-amplified interference micrograph of a single fluxon (film thickness =0.2 μm and sample temperature =4.5 K).

KT pair

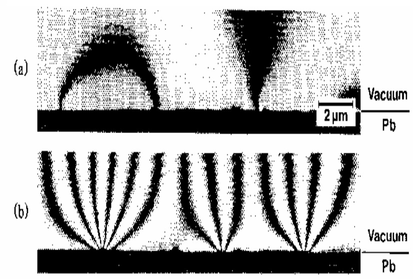

: micrographs of magnetic fluxes penetrating superconducting Pb films (phase amplification, ×2).) 1.0 μm.

Tonomura et al
PRL66,2519 (1993)

Tonomura et al
PRB43,7631 (1991)

Phase diagram

Type I

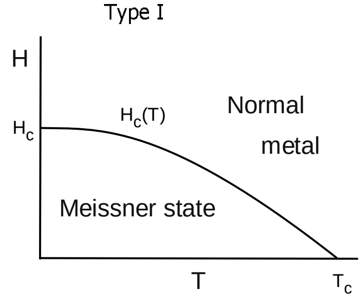

Type II

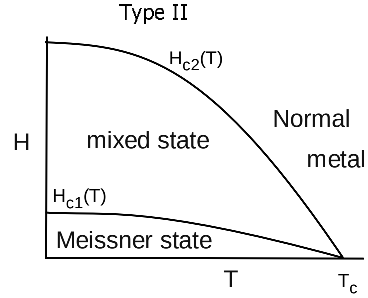

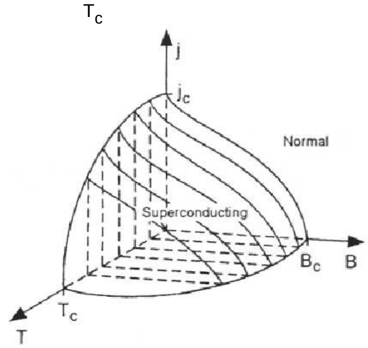

Overview of properties of vortices and systems of vortices (vortex matter)

(Adapted from Zeldov)

Inter-vortex repulsion and the Abrikosov flux line lattice

Line energy

To create a vortex, one has to provide energy per unit length (line tension)

$$\varepsilon \approx \left(\frac{\Phi_0}{4\pi\lambda}\right)^2 \log\left(\frac{\lambda}{\xi}\right)$$

Therefore vortices enter an infinite sample only when field exceeds certain value

Interactions between vortices

They interact with each other via a complicated vector-vector force. Parallel straight vortices repel each other forming highly ordered structures like flux line lattice (as seen by STM and neutron scattering).

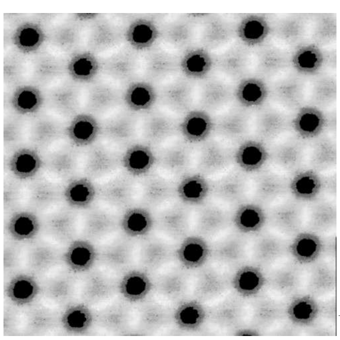

Pan et al (2002)

S.R.Park et al (2000)

Two critical fields

As a result the phase diagram of type II SC is richer than that of the two-phase type I

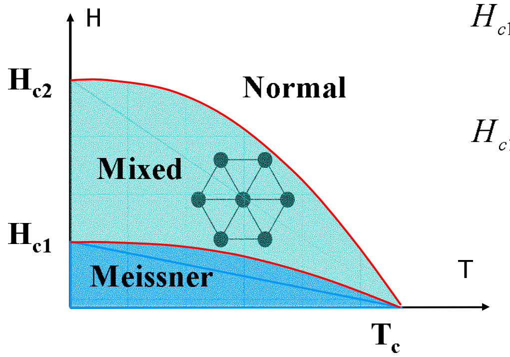

$$H_{c1} \approx \frac{\Phi_0}{4\pi\lambda^2}$$ **first vortex penetrates.**

$$H_{c2} = \frac{\Phi_0}{2\pi\xi^2}$$ **cores overlap**

$$\frac{H_{c2}}{H_{c1}} \approx \frac{2\lambda^2}{\xi^2} = 2\kappa^2 > 1$$

Two theoretical approaches to the mixed state

Just below H_{c2} vortex cores almost overlap. Instead of lines one just sees array of superconducting "islands"

Lowest Landau level appr. for constant B

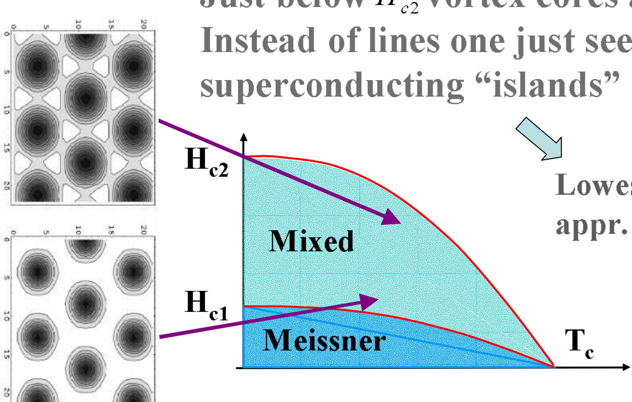

Just above H_{c1} vortices are well separated and have very thin cores

London appr. for infinitely thin lines

Thermal fluctuations and the vortex liquid

In high Tc SC due to higher **Tc**, smaller ξ and high anisotropy thermal fluctuations are not negligible. Thermally induced vibrations of the flux lattice can melt it into a "vortex liquid".

The phase diagram becomes more complicated.

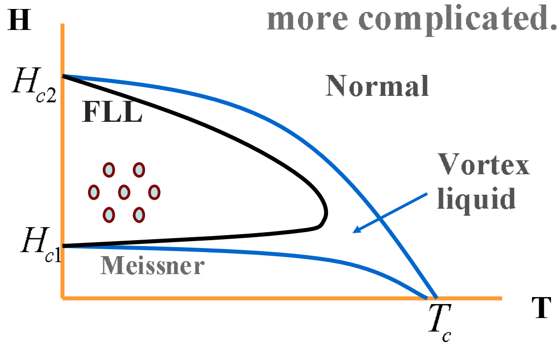

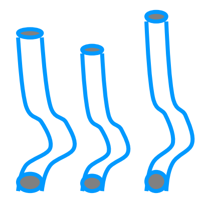

First order melting of the Abrikosov lattice

Magnetization

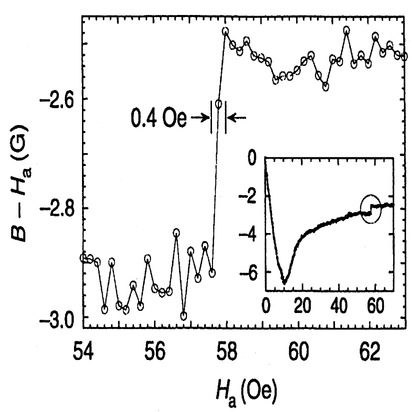

Zeldov et al
Nature (1995)

Specific heat

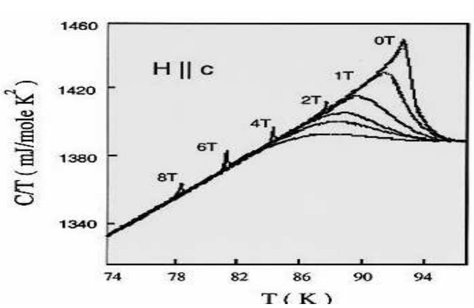

Schilling et al
Nature (1996,2001)

Thermal expansivity:

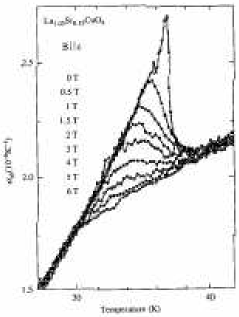

Figure D3.2.3.8. Magnetic field dependence of the in-plane thermal expansivity of a La–Sr–Cu–O single crystal in the vicinity of T_c for fields up to 6 T applied along the c-axis. (Adapted from Bruls et al [35]).

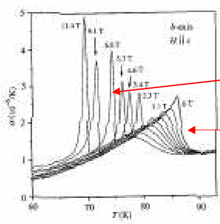

Vortex (solid-liquid) transition

SC transition

D3.2.3.9. Magnetic field dependence of the b-axis thermal expansivity of a detwinned $YBa_2Cu_3O_7$ single ... the vicinity of T_c for fields up to 11.4 T applied along the c-axis. The data show, in addition to the ... of the superconducting transition (seen also in figure D3.2.3.8), a clear signature of the irreversibility/ ... transition below T_c. (Adapted from Lortz et al [36])

Vortex "cutting" and entanglement

Vortices can entangle around each other like polymers, however due to vectorial nature of their interaction they can also "disentangle" or "cut each other".

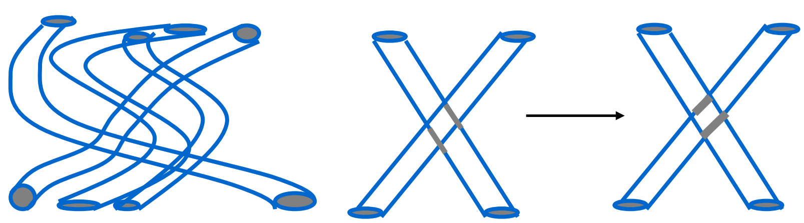

There are therefore profound differences compared to the physics of polymers

Disorder and the vortex glass

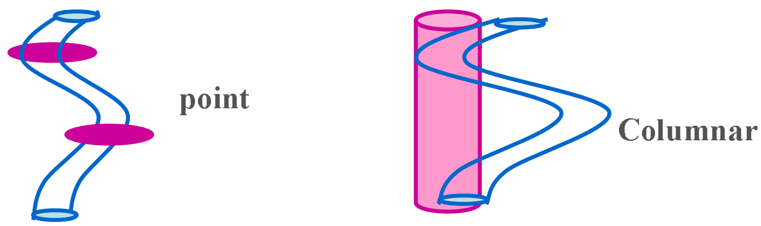

Vortices are typically pinned by disorder. For vortex systems pinning create a glassy state or viscous entangled liquid. In the glass phase material becomes superconducting (zero resistance) below certain critical current **Jc**.

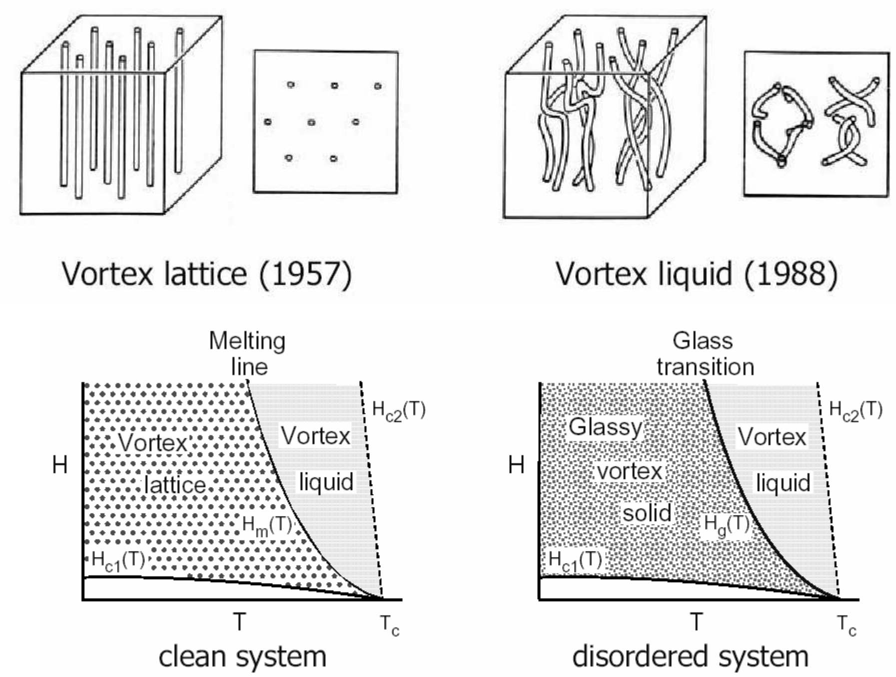

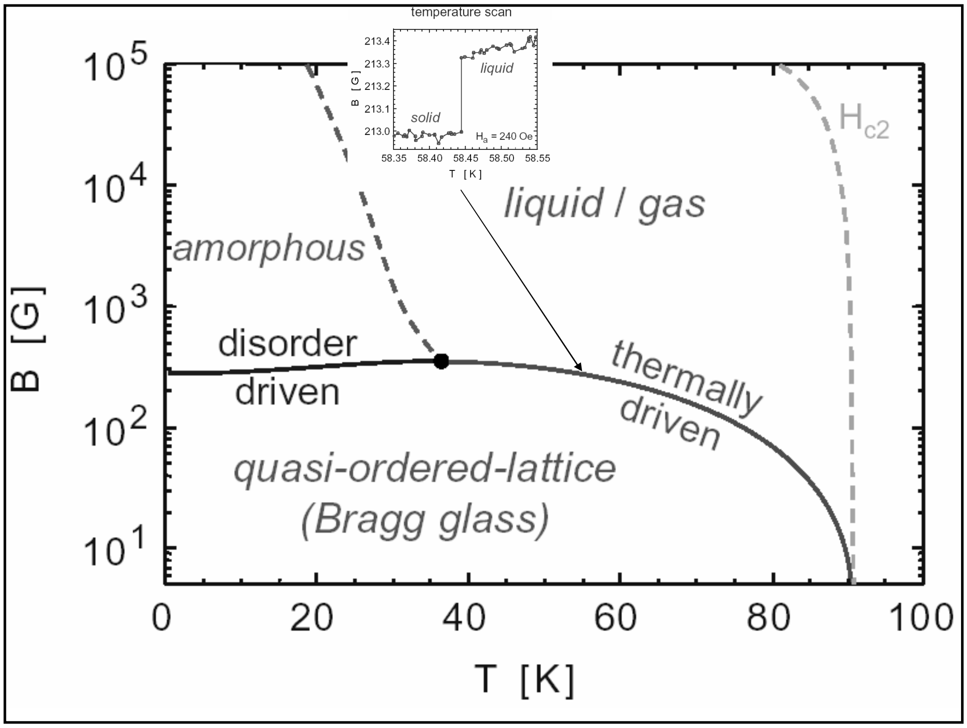

Phase diagram of low-T_c superconductors

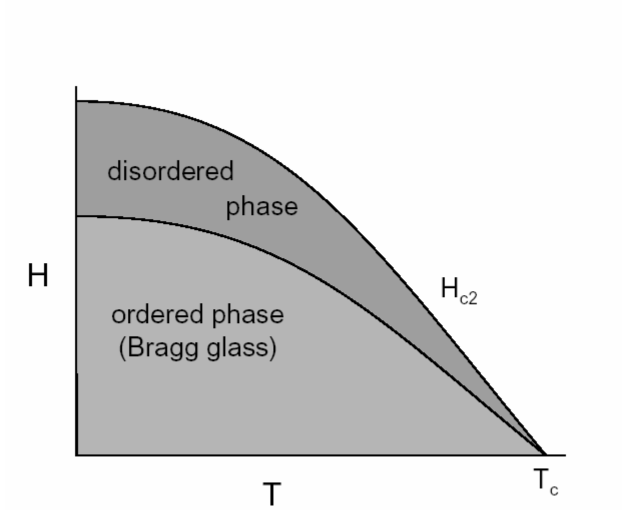

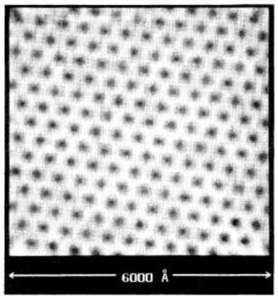

FIG. 2. Abrikosov flux lattice produced by a 1-T magnetic field in $NbSe_2$ at 1.8 K. The scan range is about 6000 Å. The gray scale corresponds to dI/dV ranging from approximately 1×10^{-8} mho (black) to 1.5×10^{-9} mho (white).

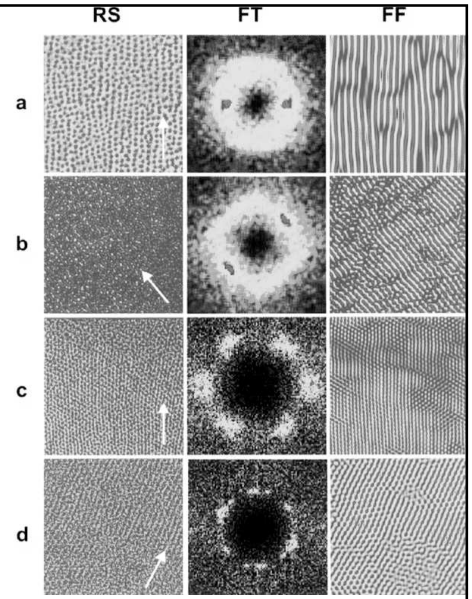

Figure 2 Images of the flux line lattice at different fields and flow velocities. Shown are real space (RS; first column) Fourier-transform space (FT; second column) and Fourier-filtered (FF; third column) images. The real-space images were digitized, flat-fielded on a 20×20 kernel and Lee filtered with a 5×5 kernel. To obtain the Fourier-filtered images, the real and imaginary components of each pixel in the Fourier-transform image were multiplied by a smooth sigmoidal function of their magnitude with a threshold of ~1/3 of the peak magnitude of the FT over the entire image. These data were then inverse-transformed and the absolute value of the inverse transform was used to construct the third column. **a**, Low-field, low-velocity data (5 Oe, 0.2 $\mu m\, s^{-1}$); **b**, low-field, high-velocity data (5 Oe, 2.5 $\mu m\, s^{-1}$); **c**, high-field, low-velocity data (20 Oe, 0.2 $\mu m\, s^{-1}$); **d**, high-field, high-velocity data (25 Oe, 3 $\mu m\, s^{-1}$). Rows **a** and **b** show a smectic vortex lattice; **c** and **d** show a moving-Bragg-glass state. The arrows in the first column show the direction of flow.

F. Pardo*, F. de la Cruz*, P. L. Gammel†, E. Bucher† & D. J. Bishop†

NATURE | VOL 396 | 26 NOVEMBER 1998 | www.nature.com

Vortex dynamics

Vortices move under influence of external current (due to the Lorentz force).

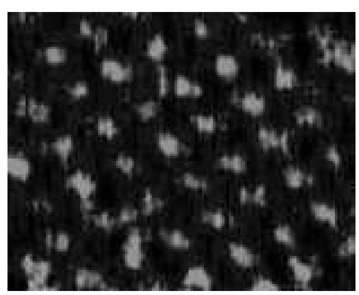

Field driven flux motion
probed by STM
on NbSe2
A.M.Troianovski (2004)

The motion is generally friction dominated. Energy is dissipated in the vortex core which is just a normal metal. The resistivity of the flux flow is no longer zero.

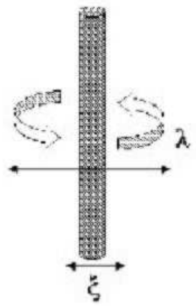

- l ~ 10000 Å
- ξ ~ 10 Å
- Hc1 ~ 100 G
- Hc2 ~ 300 T

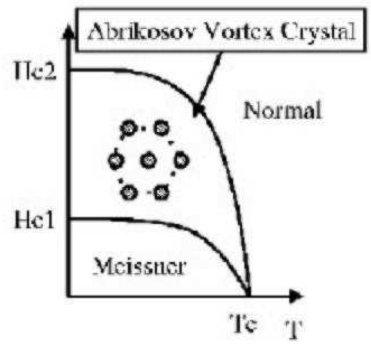

$$F \propto \begin{cases} Log(r/\xi) & r < \lambda \\ e^{-r/\lambda} & r > \lambda \end{cases}$$

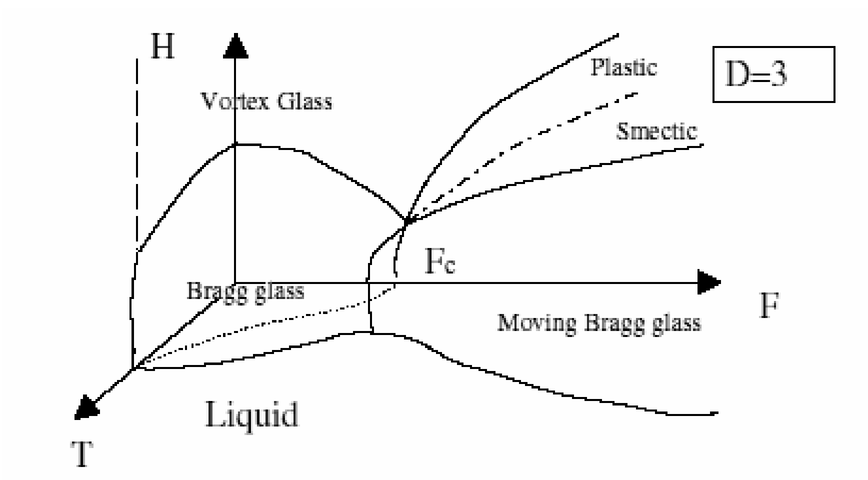

T. Giamarchi[1] and S. Bhattacharya[2]

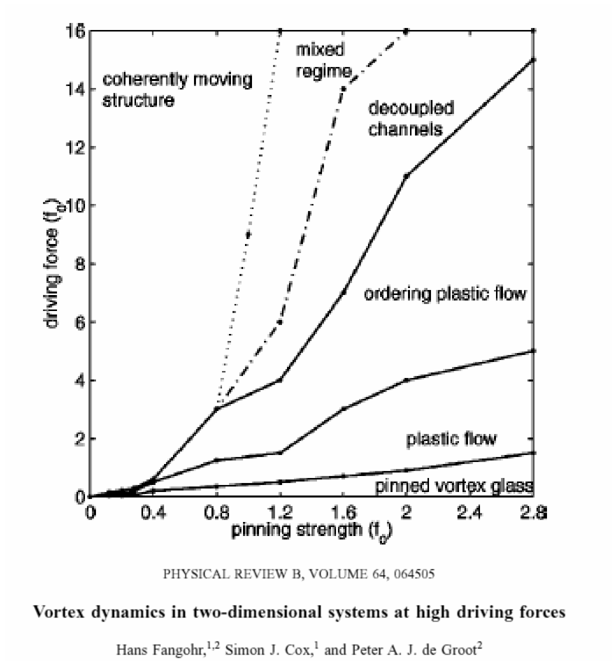

coherently moving structure
mixed regime
decoupled channels
ordering plastic flow
plastic flow
pinned vortex glass
driving force (f_0)
pinning strength (f_0)
PHYSICAL REVIEW B, VOLUME 64, 064505
Vortex dynamics in two-dimensional systems at high driving forces
Hans Fangohr,[1,2] Simon J. Cox,[1] and Peter A. J. de Groot[2]

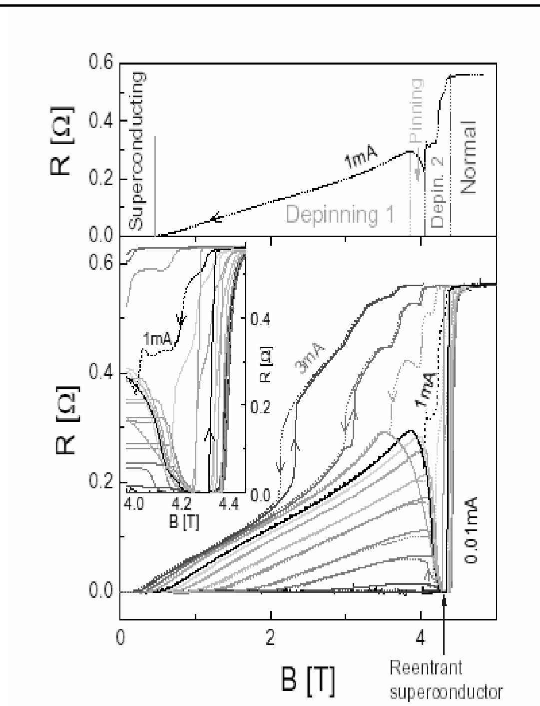

R [Ω]
Superconducting
1mA
Pinning
Depin. 2
Normal
Depinning 1
3mA
1mA
0.01mA
B [T]
Reentrant superconductor

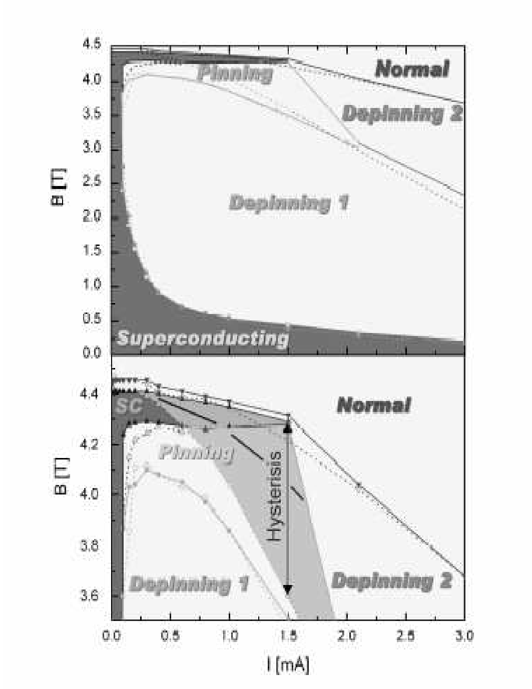

Normal
Pinning
Depinning 2
Depinning 1
Superconducting
B [T]
SC
Hysterisis
I [mA]

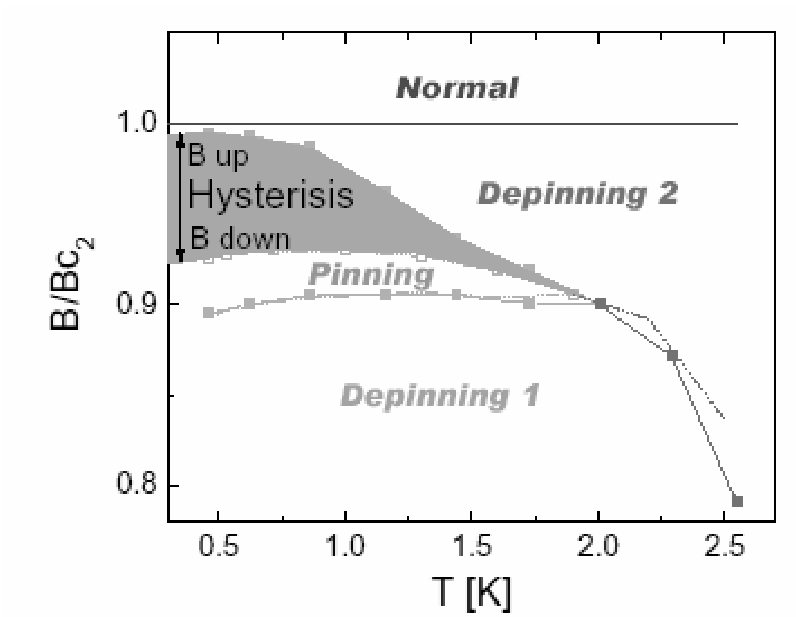

Normal
B up
Hysterisis
B down
Depinning 2
Pinning
Depinning 1
B/Bc2
T [K]

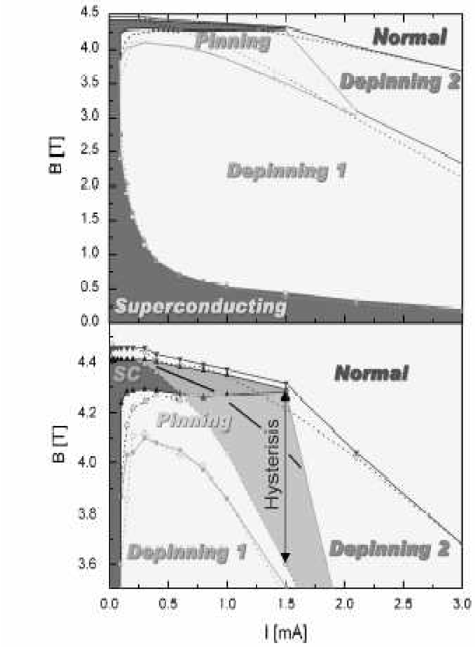
Normal
Pinning
Depinning 2
Depinning 1
Superconducting
SC
Hysterisis
Normal
Pinning
Depinning 1
Depinning 2
B [T]
I [mA]

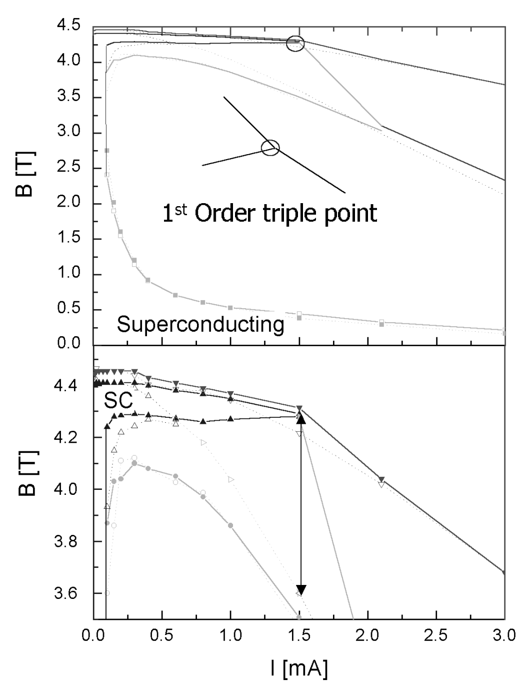
1st Order triple point
Superconducting
SC
B [T]
I [mA]

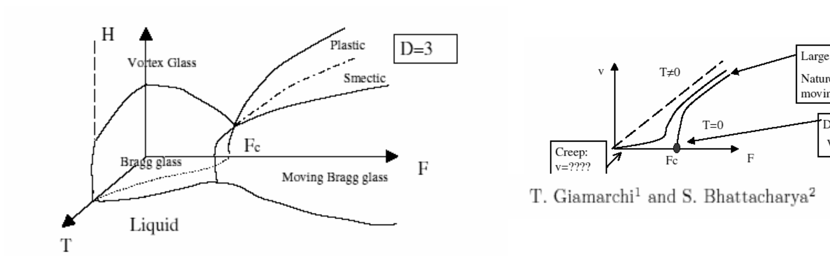

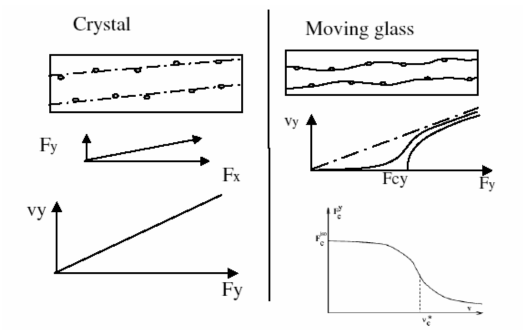

Transverse Motion

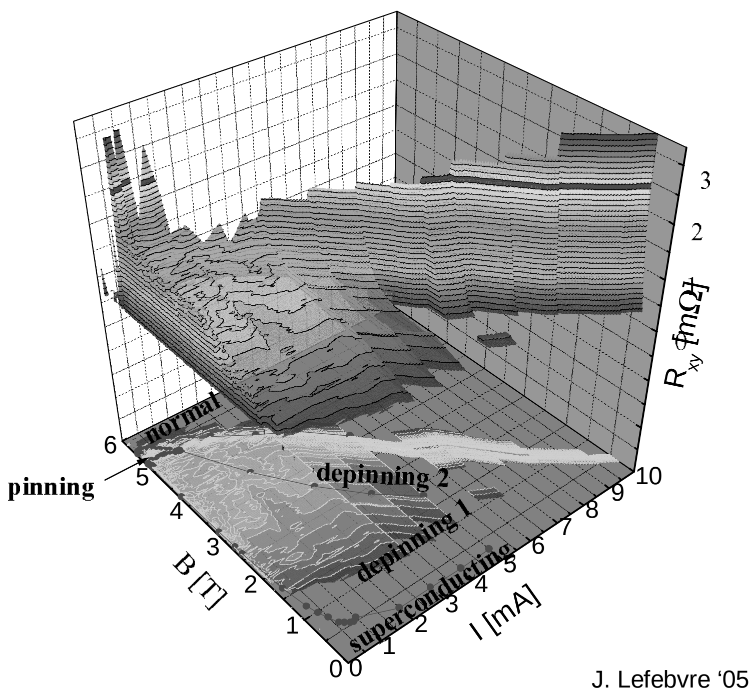

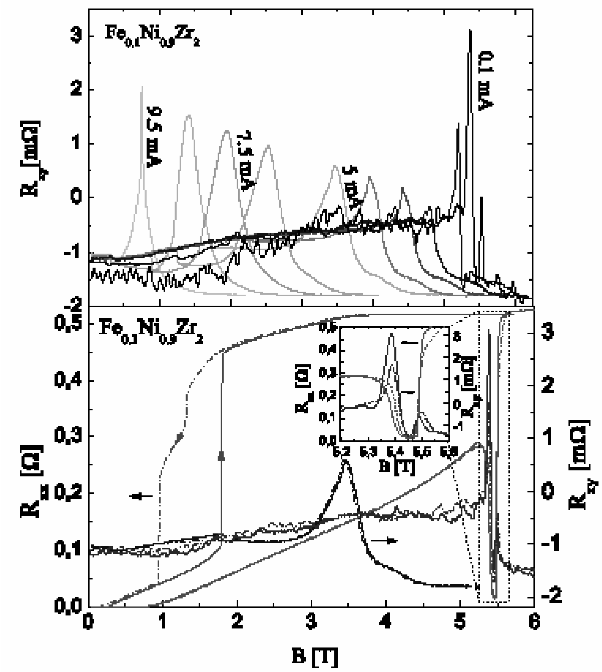

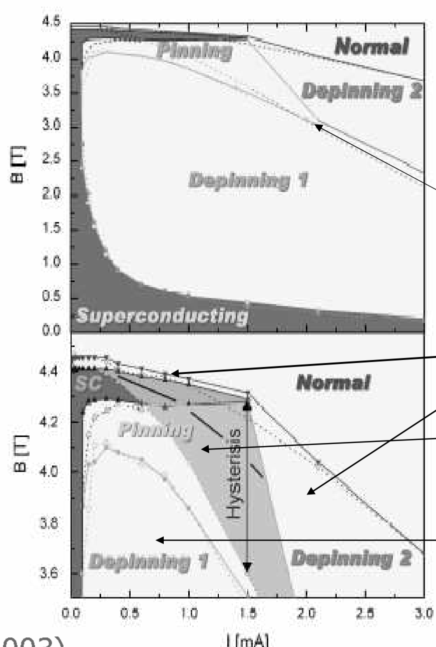

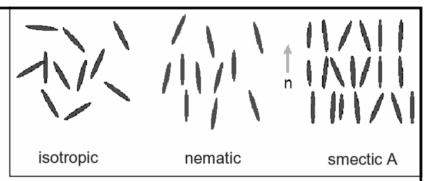

1st order phase transition (TCP)

Strong transverse motion (smectic, depinning 2)

Pinned disordered phase

Quasi-ordered phase (Bragg glass)

(2003)

Classical Phase Transitions:

Temperature driven

(Variations of Melting transition, like chocolate)

James Bay

Winter

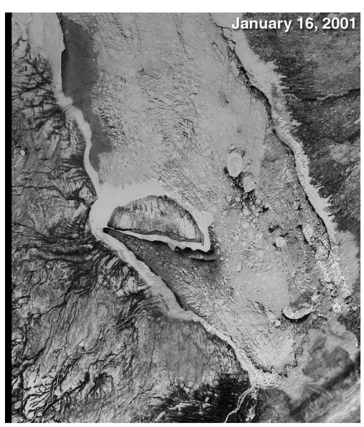

Ice

Quantum
(Ground State)

Summer

Water

Classical
(Higher temperature phases)

FIG. 1: Vortices created by air turbulence of a jet airplane.

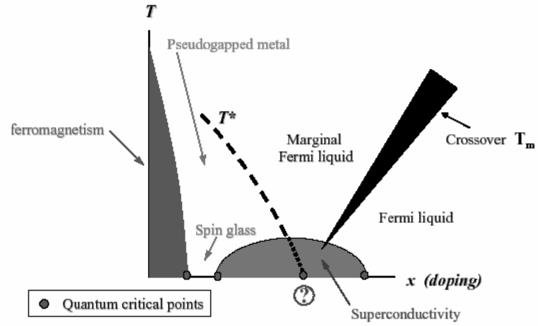

Phase diagram of high Tc superconductors

Classical vs. Quantum

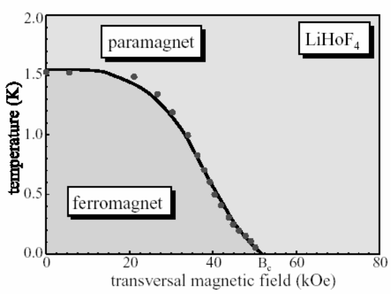

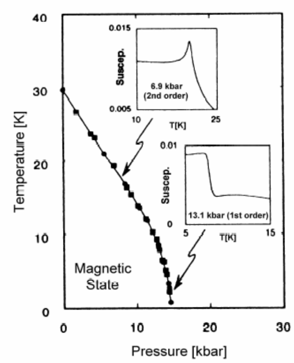

phase diagrams of $LiHoF_4$ (Bitko et al. 96) and MnSi (Pfleiderer et al. 97)

Classical partition function: statics and dynamics decouple

$$Z = \int dpdq \; e^{-\beta H(p,q)} = \int dp \; e^{-\beta T(p)} \int dq \; e^{-\beta U(q)} \sim \int dq \; e^{-\beta U(q)}$$

Quantum partition function:

$$Z = \mathrm{Tr} e^{-\beta \hat{H}} = \lim_{N\to\infty} (e^{-\beta \hat{T}/N} e^{-\beta \hat{U}/N})^N = \int D[q(\tau)] \; e^{S[q(\tau)]}$$

(Ref: Vojta)

imaginary time τ acts as additional dimension
at $T = 0$, the extension in this direction becomes infinite

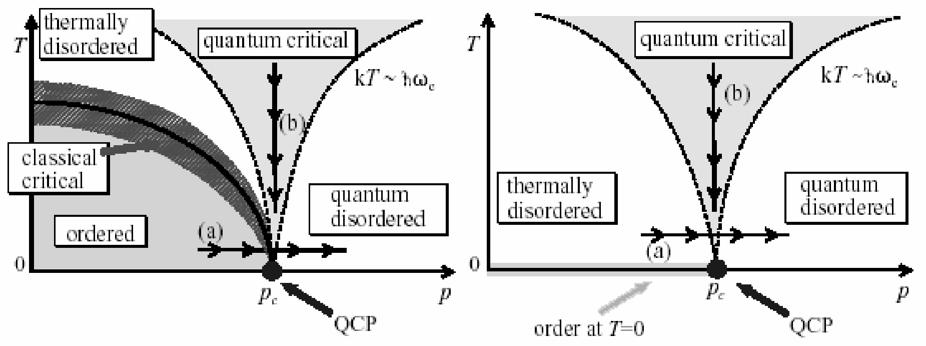

Typically power law behaviour in critical region

(Ref: Vojta)

Quantum Phase Transition: change of Ground state phase as a function of some parameter g.

g_c

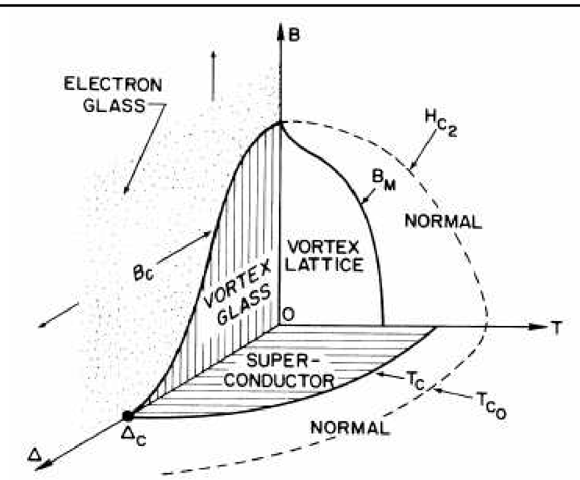

VOLUME 65, NUMBER 7 PHYSICAL REVIEW LETTERS 13 AUGUST 1990

Quantum Phase Transitions in Disordered Two-Dimensional Superconductors

Matthew P. A. Fisher

Disorder driven Quantum Phase Transition (superconductor-to-insulator transition)

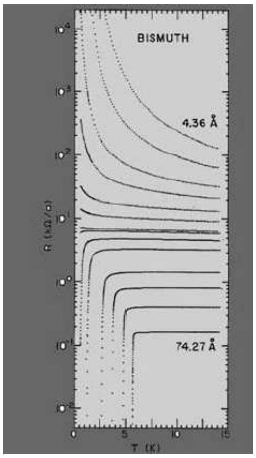

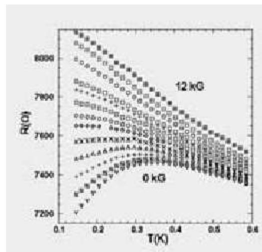

$R_{\square} = R_c F(\delta / T^{1/\nu z})$

$\nu z = 0.7$

$\delta = |H - H_c|$

$t = T^{-\nu z}$

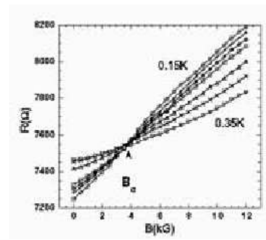

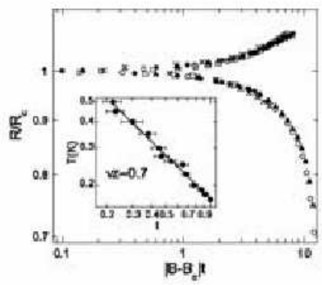

(Ref: Goldman)

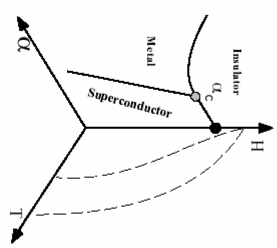

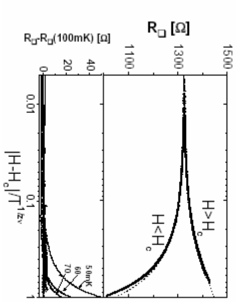

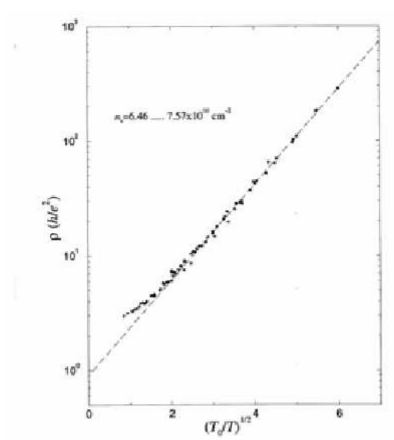

Mason *et al.* Phys. Rev. B 52, 7857 (1995)

	exponent	definition	conditions
specific heat	α	$c \propto \|t\|^{-\alpha}$	$t \to 0, B = 0$
order parameter	β	$m \propto (-t)^{\beta}$	$t \to 0$ from below, $B = 0$
susceptibility	γ	$\chi \propto \|t\|^{-\gamma}$	$t \to 0, B = 0$
critical isotherm	δ	$B \propto \|m\|^{\delta}\mathrm{sign}(m)$	$B \to 0, t = 0$
correlation length	ν	$\xi \propto \|t\|^{-\nu}$	$t \to 0, B = 0$
correlation function	η	$G(r) \propto \|r\|^{-d+2-\eta}$	$t = 0, B = 0$
dynamical	z	$\tau_c \propto \xi^{z}$	$t \to 0, B = 0$

Vojta

Quantum	Classical
d space, 1 time dimensions	$d+1$ space dimensions
Coupling constant K	Temperature T
Inverse temperature β	Finite size L_τ in "time" direction
Correlation length ξ	Correlation length ξ
Inverse characteristic energy $\hbar/\Delta, \hbar/k_B T_c$	Correlation length in the "time" direction ξ_τ

Sondhi

Interaction driven Quantum Phase Transition
(insulator-to-superconductor-to-metal transition)

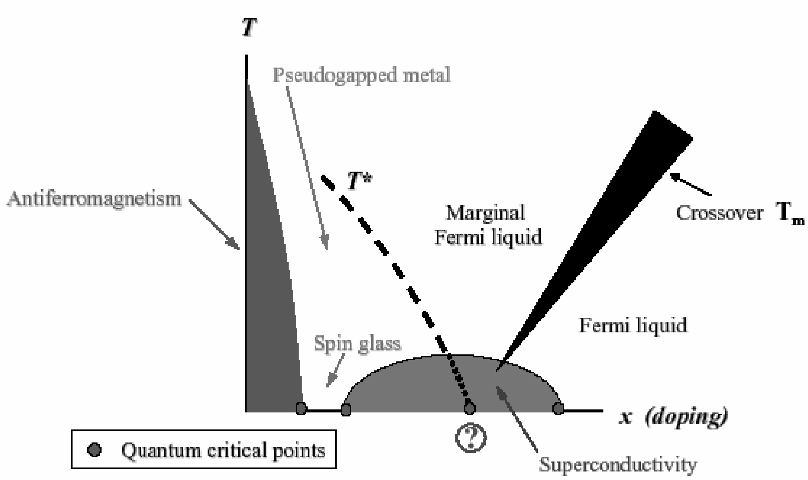

Phase diagram of high Tc superconductors

Dobrosavljevic

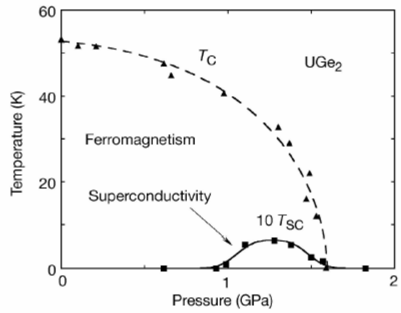

Other SC-QPTs

UGe_2, after Saxena et al., Nature 406, 587 (2000)

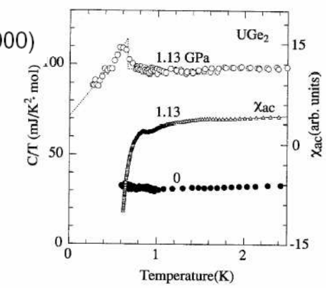

Figure 4. Temperature dependence of the specific heat in the form of C/T at 0 and 1.13 GPa, togehter with the ac susceptibility at 1.13 GPa in UGe_2.

after Tateiwa et al., J.Phys. Condens. Mat. 13, L17 (2001)

Thank you and bon appétit

Figure 1. Good and bad chocolate: The well-tempered chocolate on top is glossy and has come away easily from the mold. The untempered chocolate sticks in the mold and shows a spotted and marked surface typical of strong fat "bloom."

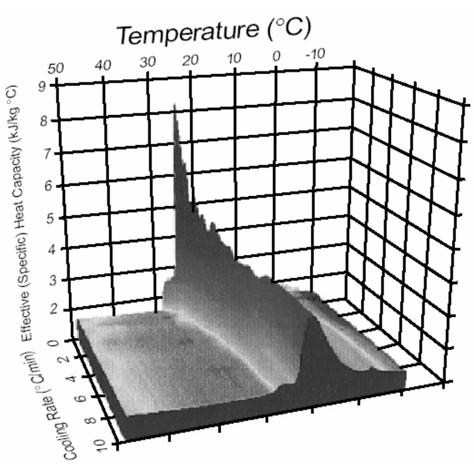

Figure 3. Effective (specific) heat capacity of milk chocolate as a function of temperature and cooling rate. Data obtained using differential scanning calorimetry. (From Reference 16.)